Acoustics Australia
https://doi.org/10.1007/s40857-024-00330-2

ORIGINAL PAPER

Numerical Simulation and Experimental Study of Aerodynamic Noise Reduction of Elbow Based on Leading- and Trailing-Edge Serrated Guide Vanes

Lili Ye[1] · Xianzhong Wang[1] · Weiguo Wu[2] · Haoran Ma[3] · Weijia Feng[1]

Received: 7 March 2024 / Accepted: 30 June 2024

Abstract
The leading-edge and trailing-edge serrated guide vanes, inspired by the silent flight of owl wings, were designed to reduce the aerodynamic noise produced by elbows in cruise. Using the acoustic finite element approach in conjunction with the large eddy simulation model, the aerodynamic noise produced by the elbow is calculated. Using an air piping test platform, this hybrid simulation technique is validated. Further simulation results showed that these two bionic guide vanes contributed to the decrease in the aerodynamic noise by streamlining the airflow and lowering the formation of laminar flow separation bubbles. In particular, the leading-edge serrated guide vane reduced noise by 4.6 dB, whereas the trailing-edge serrated guide vane reduced noise by 3.4 dB.

Keywords Cruise ship · Aerodynamic noise · Pipeline · Bionic guide vane · Noise reduction

1 Introduction

Bionics is a field of study that applies biological principles to the engineering design of artificial devices. The design of leading-edge serrations, inspired by the silent flight of owl wings and the leading-edge tubercles on humpback whale fins, has gained considerable attention. Hersh et al. [1] pioneered the study of the serrated leading-edge structure in owl wings, noting its potential to reduce aerodynamic noise in airplane wing blades by 4–5 dB. Rao et al. [2] explored the impact of the leading-edge serrations on the reduction in the aerodynamic noise using particle image velocimetry (PIV) and LES. Their findings indicated that the serrations played a pivotal role in diminishing the intensity of pressure pulsation at the blade. Drawing inspiration from low-noise flight of owls, numerous studies have proposed noise reduction designs mimicking the trailing-edge serrations [3–6]. Wang et al. [7] performed the simulation of trailing-edge serrations under the specific angle of attack using high-resolution LES combined with the acoustic analogy method. Their results showed that the overall SPL of the airfoil with serrations was reduced by 5.47 dB when compared to a smooth airfoil. Pavel and Moreau [8] applied a formal optimization technique to determine the ideal configuration of trailing-edge serrations aimed at decreasing the aerodynamic noise of a blade. Arce León et al. [9] found that a mixed solid/slit configuration had a certain benefit in noise reduction. The trailing-edge noise could be efficiently reduced by the compliant serrations. Through anechoic wind tunnel experiments, Zhou et al. [10] examined the effectiveness of flexible trailing-edge serrations of different forms for lowering airfoil self-noise. An aeroacoustics study of a NACA0012 airfoil with various modifications connected to the trailing edge (TE) at a high Reynolds number was carried out by Singh and Mimani [11, 12]. The acoustic spectra for the flaplet case revealed that at very low frequencies, self-oscillations produced tones that led to a significant increase in noise levels over baseline levels; at mid-frequencies, there was a noticeable 3–4 dB reduction in noise; and at high frequencies, there was a slight increase. Sivakumar et al. [13] presents an experimental investigation of a turbulent boundary layer interaction

✉ Xianzhong Wang
xianzhongwang00@163.com

1 School of Naval Architecture, Ocean and Energy Power Engineering, Wuhan University of Technology, Wuhan 430063, China

2 Green & Smart River-Sea-Going Ship, Cruise and Yacht Research Center, Wuhan University of Technology, Wuhan 430063, China

3 Department of Ocean Engineering, Texas A&M University, College Station, TX 77840, USA

Published online: 12 August 2024

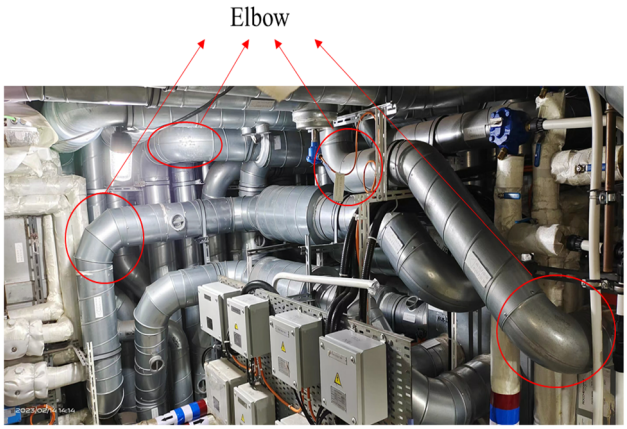

Fig. 1 Complex pipeline ventilation system on luxury cruise ships. Elbows are the most common fittings in pipeline ventilation system

over a single large triangular serration at the trailing edge (TE) of an airfoil on the flow-induced noise. It was observed that the maximum noise attenuation occurred at frequencies above 5 kHz, where the TE noise dominates over the leading-edge (LE) noise. For frequencies below 5 kHz, the LE noise sources dominate over the TE noise.

Noise pollution is a prevalent concern on cruise ships, with noise sources stemming from the ship's propulsion system, exhaust ventilation systems and onboard equipment [14–16]. As Fig. 1 shows, the ventilation piping system inside the cruise ship is complex. In luxury cruise ship superstructures, ventilation pipes are the primary contributors to noise pollution. Elbows are common fittings in air conditioning systems [17]. When air flows through an elbow, the fluid velocity near its inner edge exceeds that near the outer edge, leading to a pressure gradient [18]. Moreover, this nonuniform flow leads to the formation of eddies and vortices, which induce fluctuating pressure changes and subsequent noise generation.

Over the years, researchers have extensively explored methods to predict the aerodynamic noise in elbows through experiments and numerical simulations [19, 20]. Han et al. [21] performed CFD calculations to study the distribution of sound source and frequency spectra produced by natural gas manifolds. They also carried out a noise experiment to validate their findings. Masaaki et al. [22] delved into the acoustic pressure levels generated by airflow in a T-shaped pipe. They calculated aerodynamic noise by CAA (computational aeroacoustics).

Nowadays, the guide vane is an effective tool to mitigate the aerodynamic noise of elbows. Zhang et al. [23, 24] investigated the flow-induced noise within a 90° piping elbow and the noise reduction effect of guide vanes. Wang et al. [25] conducted an experimental study of the optimal positioning of guide vanes for minimizing flow noise in the elbow. Zhang et al. [26] found that pressure fluctuations in cases without guide vanes are much larger than those with guide vanes. Their results indicated a significant decrease in sound pressure level (SPL) when a guide vane was introduced into the elbow. Despite their efficiency, guide vanes also produce self-noise at their top and end.

Currently, while bionics research has been successfully applied in various transportation modes such as cars, high-speed railways and aircraft [27–31], its use for noise reduction in pipeline systems remains limited. This study leverages the bionic structures of owl wings and leading-edge tubercles found on humpback whale fins to design a guide vane for elbows. Both numerical simulation and experimental platform were applied to analyze the influence of the leading-edge serrations and the trailing-edge serrations on the flow field and aerodynamic noise within the elbow. The result of current study provides the basis and direction for reducing aerodynamic noise of pipelines in cruise ships.

2 Methodology

2.1 Design of Bionics

Taking inspiration from the noiseless flight of owl wings and the leading-edge tubercles found on humpback whale fins, the leading-edge serrated guide vane and the trailing-edge serrated guide vane were developed to mitigate aerodynamic noise in elbow configurations. The findings of Avallone et al. [4] suggest an optimal noise reduction when the length of the serrations is approximately twice or quadruple the boundary layer thickness. Therefore, in this study, the serration lengths are selected as 8 mm. Figure 2 illustrates the bionic design, which includes both leading-edge serrations and trailing-edge serrations. The thickness of the guide vane is denoted as a. The serration dimensions are characterized by the serration's length l, the distance between the crest and valley$h$ and the serration spacing λ. The shown positions correspond to the axial locations of the serration peaks and troughs, which are labeled as "crest" and "valley," respectively. Specifically, $h = 4$ mm, $\lambda = 3$ mm, $l = 8$ mm and $a = 2$ mm.

2.2 Computational Method

2.2.1 Turbulent Flow

In this study, the Mach number of the airflow is less than 0.3, which allows for the application of incompressible flow. The continuity equation for incompressible flow is presented as Eq. (1) [24].

$$\partial \overline{u_i}/\partial x_i = 0, \tag{1}$$

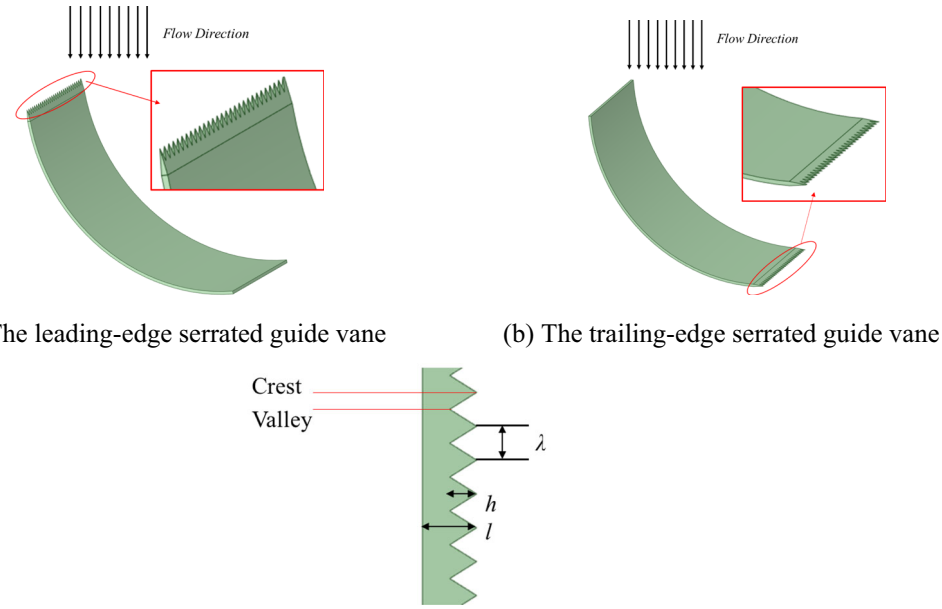

(a) The leading-edge serrated guide vane

(b) The trailing-edge serrated guide vane

(c) The design of serrations

Fig. 2 Design of the guide vane with the leading-edge serration and the trailing-edge serration

And the Navier–Stokes (N–S) equation is given in Eq. (2)

$$\frac{\partial \overline{u}_i}{\partial t} + \frac{\partial \overline{u}_i \overline{u}_j}{\partial x_j} = -\frac{1}{\rho}\frac{\partial \overline{p}}{\partial x_i} + v\frac{\partial^2 \overline{u}_i}{\partial x_i \partial x_j} - \frac{\partial \tau_{ij}}{\partial x_j}, \tag{2}$$

where ρ represents the air density, t denotes time, $\overline{p}$ stands for the time-averaged static pressure, x_i is the space coordinate and u_i and u_j are the directions of i and j [32].

Due to the substantial computational time direct numerical simulation (DNS) demands, this study employs the LES approach to calculate the air flow of the pipe. To obtain the governing equations of LES, it is necessary to apply a spatial filter to the N–S equation, which directly separates the airflow into eddies with large and small.

The influence of small-scale turbulence on the resolved scales is evident in the subgrid-scale (SGS) stress term, $\tau_{ij} = \overline{u_i u_j} - u_i u_j$, which must be modeled [33]. In this context, the Smagorinsky SGS eddy viscosity model is employed, given as

$$\tau_{ij} - \frac{1}{3}\delta_{ij}\tau_{kk} = -2\mu_t \overline{S}_{ij}, \tag{3}$$

where μ_t is the subgrid-scale eddy viscosity and $\overline{S}_{ij}$ is the strain rate tensor, respectively. And expressions of them are given as

$$\mu_t = \rho C_d \Delta^2 \left|\overline{S}_{ij}\right|, \tag{4}$$

$$\overline{S}_{ij} = \frac{1}{2}\left(\frac{\partial \overline{u}_i}{\partial x_j} + \frac{\partial \overline{u}_j}{\partial x_i}\right). \tag{5}$$

2.2.2 Acoustic Equation

The sound field calculation method is based on Goldstein's generalized Lighthill equation [34]. The equation in the frequency domain is obtained by combining the continuity and the compressible Navier–Stokes equation, and it can be expressed as:

$$\begin{aligned} c_0^2 \rho'(x, t) = &\int_{-T}^{T}\int_{S(\tau)} \rho_0 V_N' \frac{DG}{D\tau} \mathrm{d}S(y)\,\mathrm{d}\tau \\ &+ \int_{-T}^{T}\int_{S(\tau)} f_i \frac{\partial G}{\partial y_i} \mathrm{d}S(y)\,\mathrm{d}\tau \\ &+ \int_{-T}^{T}\int_{V(\tau)} T_{ij}' \frac{\partial^2 G}{\partial y_i \partial y_j} \mathrm{d}y\mathrm{d}\tau, \end{aligned} \tag{6}$$

where c_0 is the sound velocity, ρ_0 is the density of the fluid, ρ' is density disturbance caused by sound, $x = [x_1, x_2, x_3]$ is viewpoint position, $y = [y_1, y_2, y_3]$ is sound position, $c_0^2\rho'$ equal sound pressure, τ is acoustic emission time at the sound source, t is acoustic receive time at the viewpoint. G is the Green function, T_{ij}' is Lighthill's stress tensor, f_i is essentially the ith component of the force per unit area exerted by the boundaries on the fluid and V_N' is the velocity of the surface normal to itself relative to the fluid.

The first term in Eq. (6) represents sound generated by the volume displacement of a moving object, classified as a monopole sound source. The second term represents sound generated by the unsteady forces exerted by the solid surface on the fluid, classified as a dipole sound source. The third term

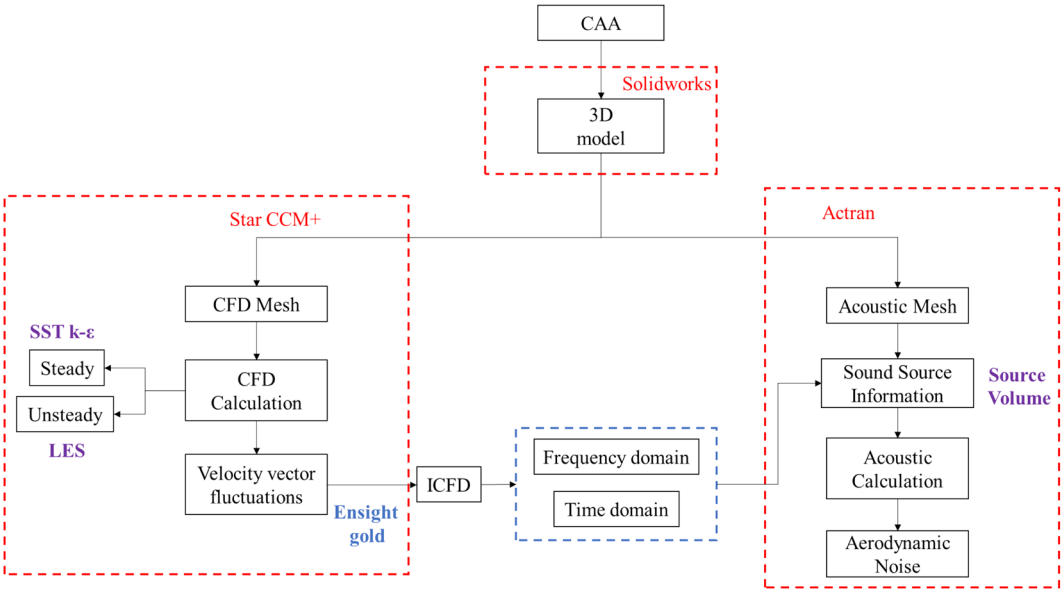

Fig. 3 Process of combined flow field/acoustic field calculation method

represents sound generated by volume sources, classified as a quadrupole sound source. Under low-Mach-number conditions, the sound produced by quadrupole sources is minimal and can usually be neglected. If the noise-generating sound source is stationary, the monopole source can also be ignored. Therefore, at low Mach numbers, the sound generated by a stationary solid in free space can be described by the following equation:

$$p(x,\, t) = \int_{-T}^{T} \int_{S(\tau)} f_i \frac{\partial G}{\partial y_i} \mathrm{d}S(y)\mathrm{d}\tau. \tag{7}$$

In the present study, we do not consider the interaction between flow and sound. Considering the interaction between flow and sound can significantly complicate both the analysis and computational aspects, it is worth noting that the Mach number of air is less than 0.3, and the impact of sound waves on the flow is minimal. Consequently, ignoring this interaction simplifies the model without significantly compromising the accuracy of the results. Sound sources are solved with finite element method.

2.3 Calculation Process

The process for aerodynamic acoustic calculation is depicted in Fig. 3. Typically, airflow noise calculations are conducted using computational aeroacoustics (CAA), which comprises two main components: CFD calculations using STAR CCM+ and sound propagation calculations by Actran. The models are imported into STAR CCM+ and Actran to establish the fluid grid and acoustic grid, respectively. Flow field calculations are conducted to acquire information about the flow within the pipe and capture the velocity vector fluctuations needed for the next step of the calculations. Steady calculations are employed prior to unsteady calculations. The Realizable k-ε model is utilized for the steady calculations, while LES is applied for the unsteady calculations. Subsequently, ICFD (Interface CFD) serves as the bridge between STAR CCM+ and Actran, outputting the Lighthill sound sources volume in the frequency domain on the acoustic mesh. Finally, calculations for sound propagation are performed using the finite element method.

For sound field analysis in this research, the frequency range spans from 10 Hz to 1 kHz. So, to meet the stability of the calculation, the time step is configured to be 1×10^{-4} s. And the number of calculation steps is 5000, the maximum iteration limit for each time step is set as 20.

In the confined flow, there will be significant flow induced pressure fluctuations, which will in turn drive acoustic waves. These acoustic waves will couple with the pipe modes and form the flow-excited noise. As shown in manuscript [35], the sound pressure level of flow-excited noise is substantially lower than that of flow noise. Therefore, flow-excited noise is not considered here.

2.4 Geometric Model

A three-dimensional elbow is depicted in Fig. 4. The elbow has a circular cross section with a 85 mm diameter (D). The length of the inlet and outlet is 5*D* and 10D, respectively, and the elbow's radius of curvature is 1.5*D*. The computational domain and boundaries are also shown in Fig. 4. The inlet boundary condition has been set to uniform speed, while the outlet boundary assumes a pressure boundary condition at a

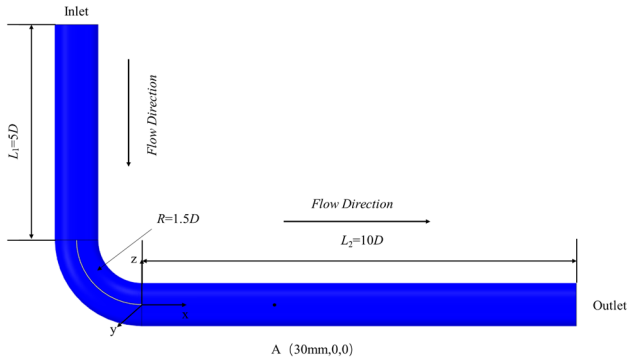

Fig. 4 The computational domain for the elbow includes the boundary conditions, the location of the monitoring point and the direction of flow

relative pressure of 0 Pa. The elbow surfaces and guide vane surfaces are treated as no-slip walls. Taking the end of the guide vane as the origin, the downstream airflow direction is the x-axis, and the upstream airflow direction is the z-axis. The flow field symmetry plane is defined as the xz plane. To analyze the aerodynamic noise of the elbow, deploy a monitoring point A with the coordinate (30 mm,0,0).

2.5 Grid Independence Verification

This study utilizes a prismatic layer mesh for the surfaces of the three elbows and the guide vanes. Meanwhile, polyhedral meshes are employed to discretize the model, enhancing the computational efficiency. To accurately capture the detailed flow characteristics near the elbow and serrated guide vane, the first layer's mesh size is configured to be less than 1.7 $\times$ 10^{-5} m to ensure $y^+ < 1$. Additionally, a growth rate of 1.2 is used and 20 prism layers are generated to cover the boundary layer thickness. For the guided vane tail, a refined mesh is employed to precisely determine airflow information (Fig. 5).

The choice of grid size in calculations can influence the accuracy and efficiency of numerical results. To verify grid independence, simulations were run on four grid resolutions with varying numbers of fluid domain grids, under an inflow velocity of 20 m/s. These numbers are 6 $\times$ 10^6, 8 $\times$ 10^6, 1 $\times$ 10^7 and 1.2 $\times$ 10^7. Simulations of the overall sound pressure level are conducted using these grids, and the results are given in Table 1. This table reveals that as the number of cells increases, the overall sound pressure level rises from 114.3 to 114.8 dB, then 115.2 dB and 115.3 dB. Considering on a balance between accuracy and computational efficiency, the total cell number of 1 $\times$ 10^7 is chosen.

Table 1 Verification of grid independence

	Total cells	Overall sound pressure level (dB)
1	6 $\times$ 10^6	114.3
2	8 $\times$ 10^6	114.8
3	1 $\times$ 10^7	115.2
4	1.2 $\times$ 10^7	115.3

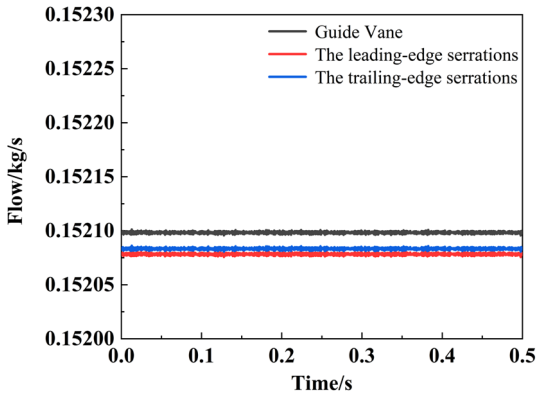

Fig. 6 Convergence analysis of fluid field calculations

Flow monitoring points are placed at the model's outlet. As shown in Fig. 6, there is virtually no fluctuation in the flow at the bent pipe's outlet when using the leading-edge serrated guide vane, the trailing-edge serrated guide vane or the conventional guide vane. This proves that the mesh

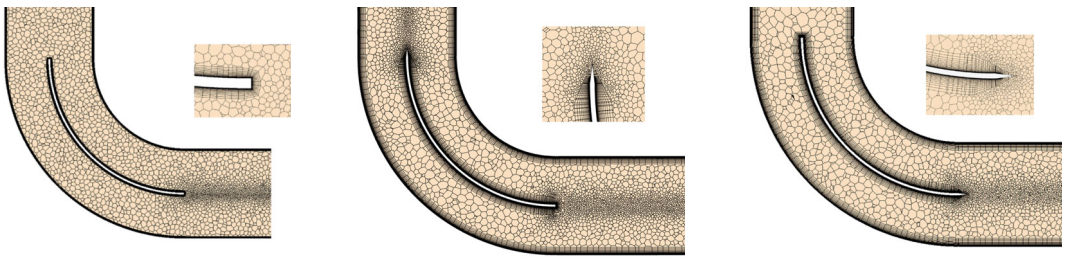

(a) The normal guide vane

(b) The leading-edge serrated guide vane

(c) The trailing-edge serrated guide vane

Fig. 5 Fluid meshing of the elbow with the normal guide vane, the leading-edge serrated guide vane and the trailing-edge serrated guide vane

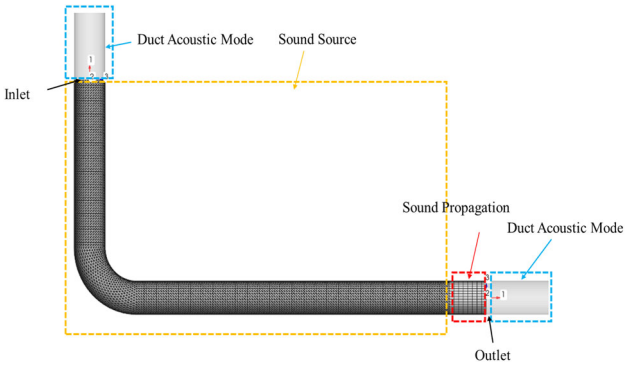

Fig. 7 The acoustic calculation domain includes: duct acoustic mode, sound source, sound propagation

quality satisfies the computational requirements by showing that the fluid computations have attained convergence.

2.6 Acoustic Calculation Domain

As shown in Fig. 7, the acoustic computational domain of the elbow is primarily divided into three regions: the sound source domain, the propagation domain and the pipeline acoustic mode regions. The area marked with red dashed lines represents the acoustic propagation domain. The area marked with yellow dashed lines in Fig. 7 represents the sound source set as the Lighthill volume. The area marked with blue dashed lines in the figure represents the pipeline acoustic mode boundary conditions set at the inlet and outlet of the pipe, used to simulate an infinitely long pipeline.

2.7 Experiment and Simulation Verification

As shown in Fig. 8, the experimental platform was designed to verify the CAA method's accuracy and evaluate the serrated guide vanes' effectiveness in reducing aerodynamic noise in the ventilating pipe system. The experimental setup included a centrifugal fan, plenum chamber, valve, muffler, shock absorber throats and other components. The power of the centrifugal fan is 0.55 kW, the max flow rate is 1100 m^3/h and the max rotational speed is 2900 r/min. The noise produced by the centrifugal fan is muffled by a plenum chamber. To lessen vibration transmission, rubber shock absorber mouths are fitted at the valve's input and exit. To lessen noise propagation in the pipeline, a muffler is positioned in front of the measurement area. A nonreflective boundary condition is created at the system's end by an additional muffler. The support frame's bottom is filled with rubber to dampen pipe vibration.

The diagram of the test instrument connection is displayed in Fig. 9a. The microphone should be mounted on the pipe's wall rather than inside of it to reduce its effect on the flow of air within the pipe. Since the pipe wall's hole diameter is greater than the microphone's, air leakage is unavoidable.

Fig. 8 Schematic diagram of the experimental setup: fan, muffler, bracket, etc. Photograph of the experimental setup

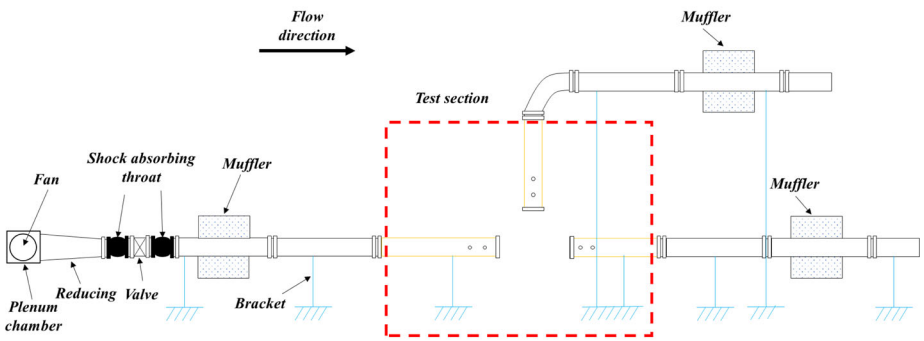

(a) The schematic illustration of the air duct testing system

(b) The photograph of the pipeline test system

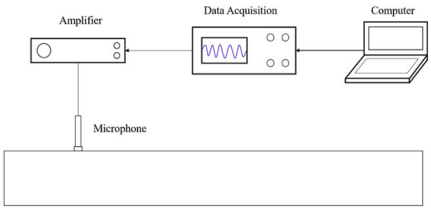

(a) Test instrument connection

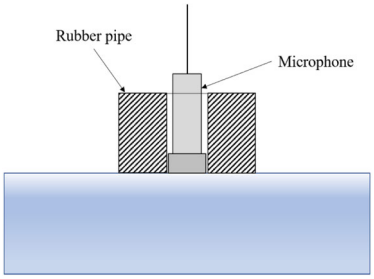

(b) Installation diagram of microphone

(c) Installation of microphone

Fig. 9 Schematic diagram and the photographs of the experimental instruments and the installation of the microphone

Table 2 Measurement results of background noise

Background noise	1	2
Results (dB)	120.1 dB	116.3 dB

In order to lessen this, as illustrated in Fig. 9b, c, we placed the microphone within a rubber tube and covered it with aluminum foil. This method lessens interference from outside noise sources and stops air leakage noise during experimental measurements. In Table 2, the background noise is shown by Result 1 for the case when the fan starts without the measure and Result 2 for the case when the fan starts with the measure.

As depicted in Fig. 10a, the thickness of the elbow and the guide vane was 2 mm, with the guide vane welded at the center of the elbow. The elbows with the serrated guide vane were manufactured through 3D printing technology using plastic and the thickness was 2 mm too, as shown in Fig. 10b. The airflow speed was controlled by a frequency converter that adjusted the fan's velocity, ensuring the airflow rate at the elbow inlet met the test requirements of 20 m/s.

Figure 11 illustrates that the main noise energy from elbow with leading-edge serrated guide vane and trailing-edge serrated guide vane is concentrated in the frequency range spanning from 0 to 5000 Hz. The main sound energy is particularly concentrated in the low-frequency range, especially within the range of 0–100 Hz. Beyond 100 Hz, the spectral curve of sound pressure levels in elbows with conventional guide vanes, leading-edge serrated guide vanes and trailing-edge serrated guide vanes shows a decreasing trend. This phenomenon is consistent with the sound pressure level curve characteristics of a ship's piping system. Both leading-edge serrated guide vane and trailing-edge serrated guide vane can reduce noise in the frequency range between 0 and 5000 Hz. As indicated by the curves, the sound pressure level in the frequency range of 1000–5000 Hz is lower than that within the 10–1000 Hz range. Therefore, our primary focus in the actual analysis lies within the frequency range from 10 to 1000 Hz. The sound pressure level (SPL) curves of all guide vanes exhibit a peak at 42 Hz, as illustrated in Fig. 11. Considering the vortex shedding frequency formula (8) [36],

$$f = \mathrm{Sr} \times V/D. \tag{8}$$

where Sr is Strouhal number, when the Reynolds number is between 300 and 3×10^5, and the Sr is approximately a constant value of 0.21. The Reynolds number for the operating condition in this manuscript is 1.2×10^5. V is inflow velocity which is 20 m/s in this manuscript. D is the windward width of the blunt body which is 85 mm in this manuscript. The calculated vortex shedding frequency is 49.4 Hz. This confirms that the peak value at 42 Hz is indeed caused by vortex shedding.

As depicted in Fig. 11c, compared to the trailing-edge serrated guide vane, the leading-edge serrated guide vane shows noise reduction in the 10–30 Hz range. Conversely, the trailing-edge serrated guide vane outperforms the leading-edge serrated guide vane in noise reduction within the 40–125 Hz range.

As given in Table 3, the leading-edge serrated guide vane can notably lower by as much as 4.6 dB across the 0–5000 Hz frequency range. Similarly, the trailing-edge serrated guide vane can lower by up to 3.4 dB within the 0–5000 Hz range.

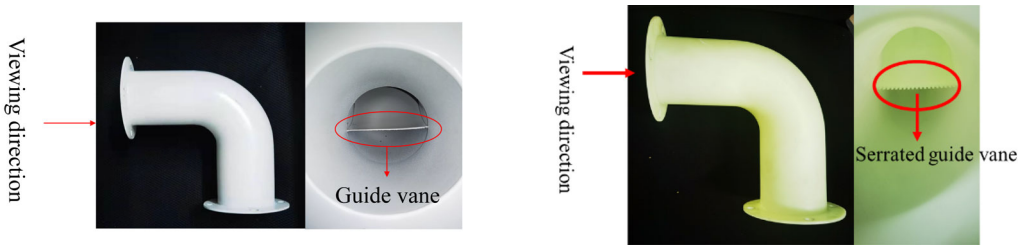

(a) The elbow with guide vane (b) The elbow with serrated guide vane

Fig. 10 Test specimen of the elbow with normal guide vane and the elbow with serrated guide vane

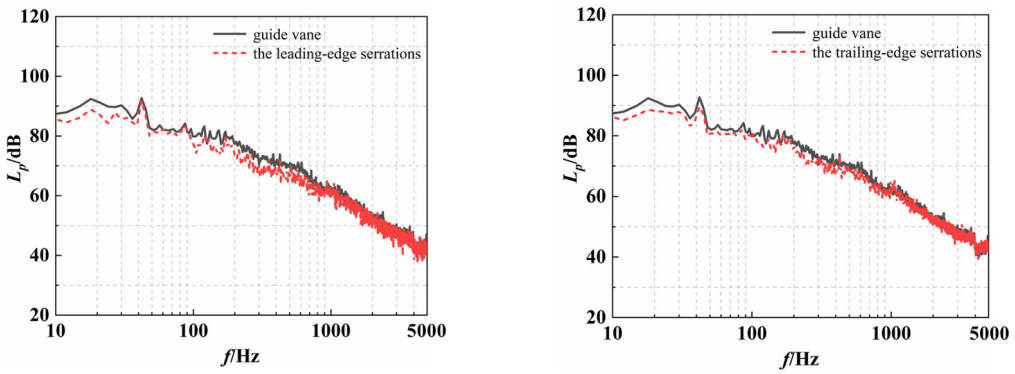

(a) The elbow with the leading-edge serrated guide vane (b) The elbow with the trailing-edge serrated guide vane

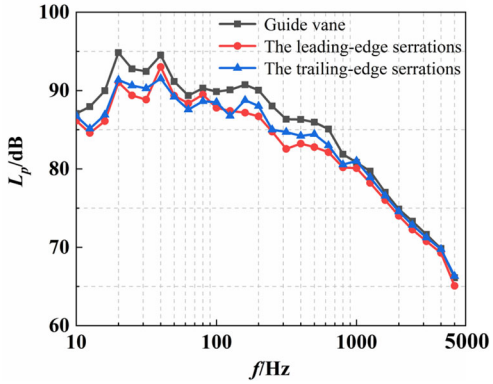

(c) The 1/3 octave band frequency spectrum

Fig. 11 Comparison between the elbow with standard guide vane spectral and the serrated guide vane spectral

Table 3 Comparison of the overall sound pressure levels

Case	Overall sound pressure level (dB)
Normal guide vane	116.3
Guide vane with leading-edge serrations	111.7
Guide vane with trailing-edge serrations	112.9

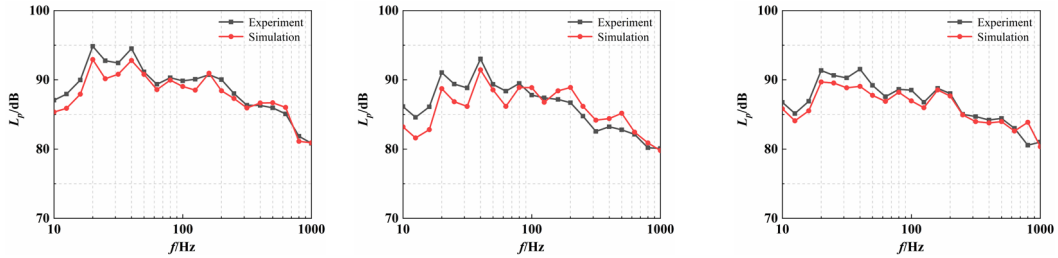

(a) The normal guide vane (b) The leading-edge serrated guide vane (c) The trailing-edge serrated guide vane

Fig. 12 Comparison of the numerical and experimental analysis of the elbow with the normal guide vane, the leading-edge serrated guide vane and the trailing-edge serrated guide vane in 1/3rd octave band

Table 4 Comparison of overall sound pressure levels between numerical and experimental analysis

Case	Experiment results (dB)	Simulation results (dB)	Error percentage (%)
Normal guide vane	116.3	115.2	0.95
Guide vane with leading-edge serrations	111.7	110.5	1.07
Guide vane with trailing-edge serrations	112.9	111.6	1.15

Comparative analysis of the experimental and numerical results from the monitoring points reveals that at an inlet flow rate of 20 m/s, the noise sound pressure level curves of 1/3 octave band exhibit similar trends, as shown in Fig. 12. This agreement between simulated and experimental results validates the reliability of numerical simulation as an accurate method for calculating aerodynamic noise produced by elbows fitted with both leading-edge and trailing-edge serrated guide vanes. Additionally, Fig. 12 demonstrates that the noise displayed a broadband spectrum in both the simulated and experimental results. Due to the influence of ambient noise and the noise generated by the operation of the fan, the experimental results are generally higher than the numerical results.

Table 4 presents a minimal difference between numerical and experimental outcomes. Specifically, the discrepancy for the standard guide vane is merely 0.95%. For the guide vane with leading-edge serrations, the difference is slightly higher at 1.07%. Lastly, the guide vane with trailing-edge serrations exhibits a discrepancy of 1.15%.

3 Results and Analysis

3.1 Flow Field Analysis

The guide vane inside the elbow extends inward to redirect the fluid flow. As air passes through the guide vane, it experiences pressure variations that induce a backward flow, generating a secondary flow field. This process leads to the formation of vortices both upstream and downstream of the guide vane. According to vortex sound theory, these vortices serve as the sole and primary source of radiated sound fields under low Mach numbers. Therefore, optimizing the flow fields both upstream and downstream of the guide vane presents an effective method for optimizing aerodynamic noise.

Distinct differences can be observed in the velocity vector contours among the three types of guide vanes. As shown in Fig. 13a–c, two vortices are apparent on each side of the front section of both the standard and trailing-edge serrated guide vanes. Additionally, obviously laminar separation bubbles can be seen at the tip of the guide vane. These bubbles have the potential to evolve into separation eddies and may eventually detach from the guide vane. In contrast, the leading-edge serrated guide vane exhibits minimal vortices at its tip, indicating that the leading-edge serrations effectively mitigate the formation of laminar flow separation bubbles.

Figure 13d–f illustrates that both the red and green regions on either side of the leading-edge serrations guide vane are smaller in area compared to those of the other two guide vanes. This observation implies that the leading-edge serrated guide vane can disperse the airflow more uniformly across the top and sides of the guide vane.

Figure 13g–i depicts two vortices of disparate scales located downstream of the guide vane, near the elbow's interior side. The lengths of these vortices are 0.019 m and 0.025 m, respectively. In contrast, the leading-edge serrations guide vane hosts a single, small-scale vortex center with a vortex length of 0.017 m. The trailing-edge serrations guide vane

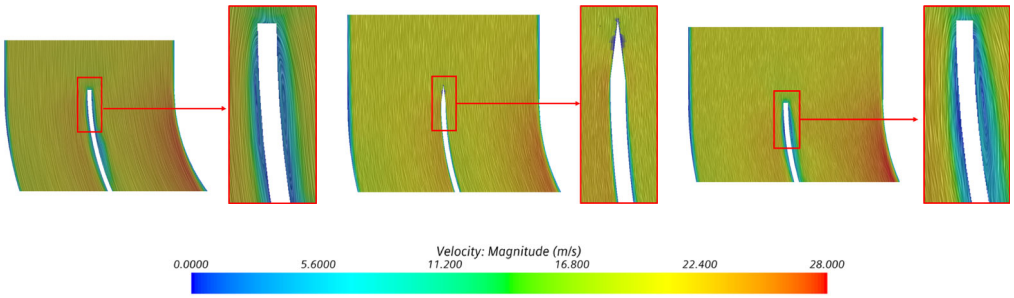

(a) Normal guide vane (b) The leading-edge serrated guide vane (c) The trailing-edge serrated guide vane

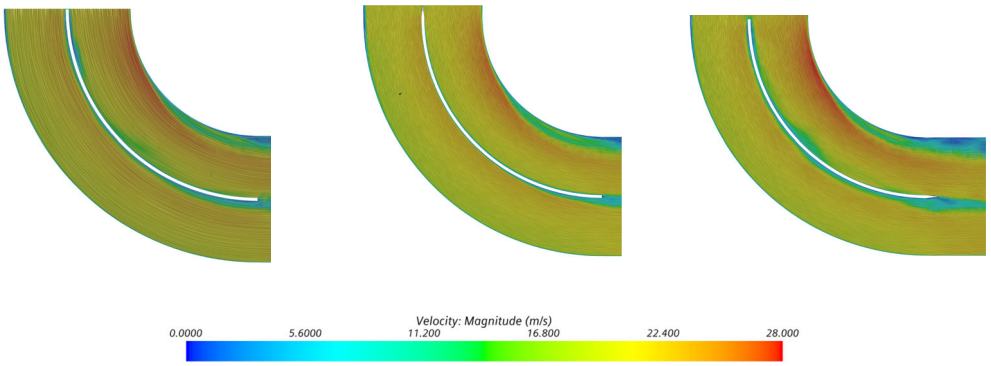

(d) Normal guide vane (e) The leading-edge serrated guide vane (f) The trailing-edge serrated guide vane

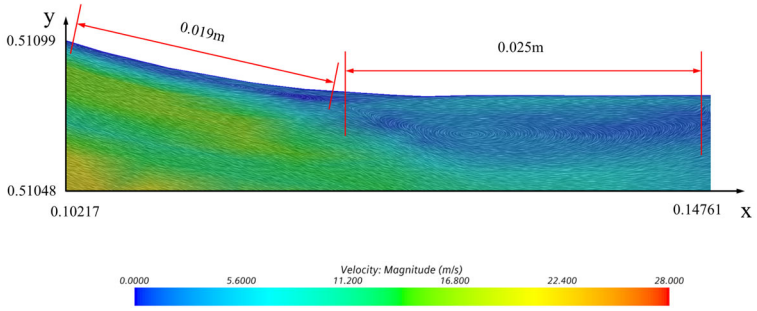

(g) Normal guide vane

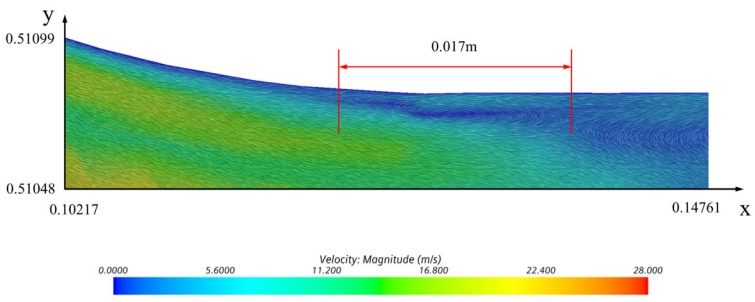

(h) The leading-edge serrated guide vane

Fig. 13 Velocity vector contour of the elbows with the normal guide vane, the leading-edge serrated guide vane and the trailing-edge serrated guide vane in different parts

Fig. 13 continued

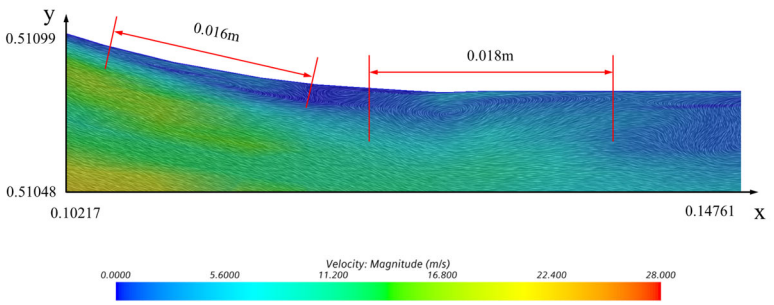

(i) The trailing-edge serrated guide vane

contains two large-scale vortices and one small-scale vortex, with lengths of 0.016 m and 0.018 m, respectively.

The analysis suggests that both bionic structures contribute to streamlining airflow within the elbow and reducing the formation of laminar flow separation bubbles. The presence of vortices, at both the tip of the leading-edge serrated guide vane and downstream of the trailing-edge serrated guide vane, is diminished. According to vortex sound theory, aerodynamic noise originates from vortices. Therefore, a decrease in vortex size, both at the guide vane's tip and downstream, facilitates a reduction in the elbow's aerodynamic noise. Thus, the leading-edge and trailing-edge serrated guide vanes positively influence the mitigation of aerodynamic noise.

To quantitatively measure the influence of velocity within the pipe, a flow uniformity index, denoted as γ has been introduced [37]. The calculation formula for the flow uniformity index is shown in Eq. (9).

$$\gamma = 1 - \frac{1}{2n} \sum_{i=1}^{n} \frac{\sqrt{(v_i - \overline{v})^2}}{\overline{v}} \tag{9}$$

where v_i represents the flow velocity in i, $\overline{v}$ denotes the mean flow velocity in the pipe and n signifies the number of nodes on a specific cross section. A higher uniformity index signifies a more uniform flow field.

The uniformity index γ of elbows with the guide vane, the leading-edge serrated guide vane and the trailing-edge serrated guide vane is shown in Fig. 14. $L_{\text{pipe}}/D = 0$ means the cross section at the trailing edge of the guide vane, and $L_{\text{pipe}}/D = 10$ means the outlet cross section of the elbow.

Both the uniformity indices for the elbows with the leading-edge serrated guide vane and the trailing-edge serrated guide vane are larger than that for the elbow with the standard guide vane. This suggests that the bionic structure can streamline the airflow inside the elbow.

The pressure contours on both sides of the guide vanes illustrate the pressure gradient. As airflow moves from a

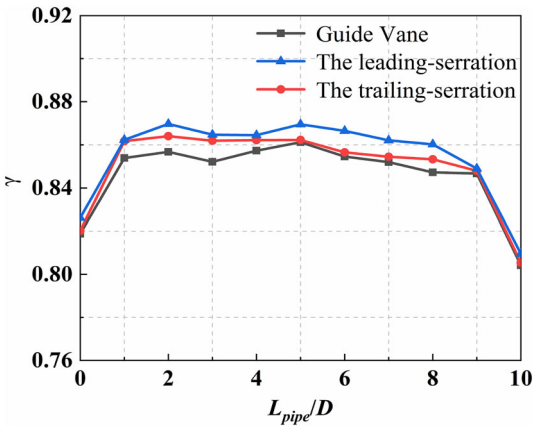

Fig. 14 Uniformity index of elbows with the normal guide vane, the leading-serrated guide vane and the trailing-serrated guide vane

region of lower pressure to one of higher pressure, it encounters an adverse pressure gradient. This requires the airflow to overcome the opposing force, thus reducing its velocity. Some airflow, unable to overcome this adverse gradient, results in backflow, leading to vortex formation. The center of this lower-pressure region is crucial in vortex formation. Consequently, the location of negative pressure is a critical determinant in the elicitation of aerodynamic noise, with the differential pressure supplying the centripetal force essential for vortex motion [38]. Figure 15a, b reveals the presence of a high-pressure region on the top of the guide vane, which is seen to disappear upon the addition of the leading-edge serrated guide vane. There is a negative pressure center above the inner wall in the pressure contour. It becomes evident that the negative pressure area, located above the inner wall of both the leading-edge and trailing-edge serrations guide vane, is notably reduced, subsequently diminishing the vortex intensity above the inner wall.

Turbulent kinetic energy (TKE) is an indicator of the energy contained within turbulent eddies or vortices in a fluid. The higher the TKE, the more intense the turbulence and thus the greater potential for aerodynamic noise generation. Figure 16a, b shows that the TKE at the top and sides of the

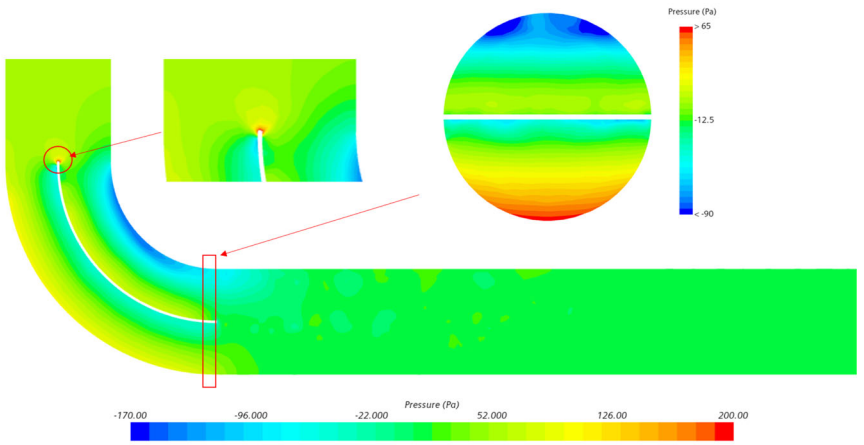

(a) The normal guide vane

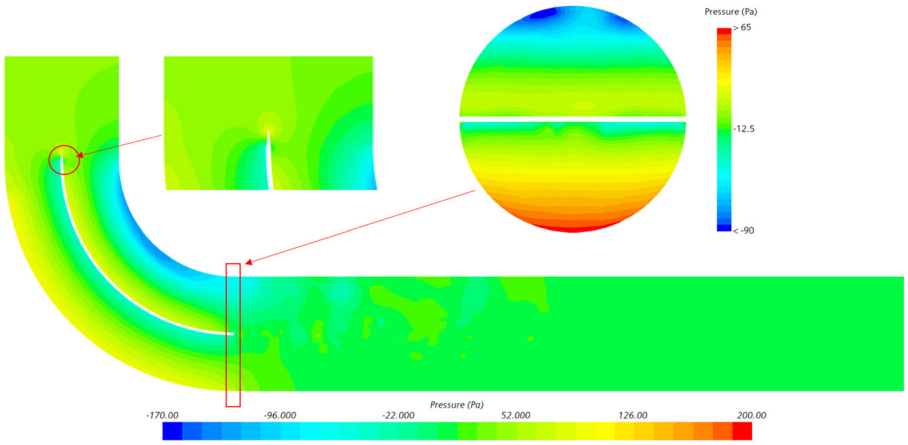

(b) The leading-edge serrated guide vane

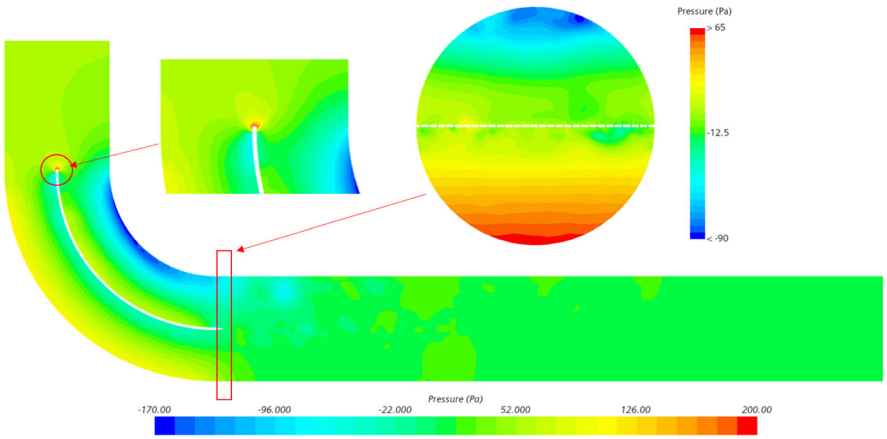

(c) The trailing-edge serrated guide vane

Fig. 15 Pressure contours of the elbows with the normal guide vane, the leading-edge serrated guide vane and the trailing-edge serrated guide vane in different parts

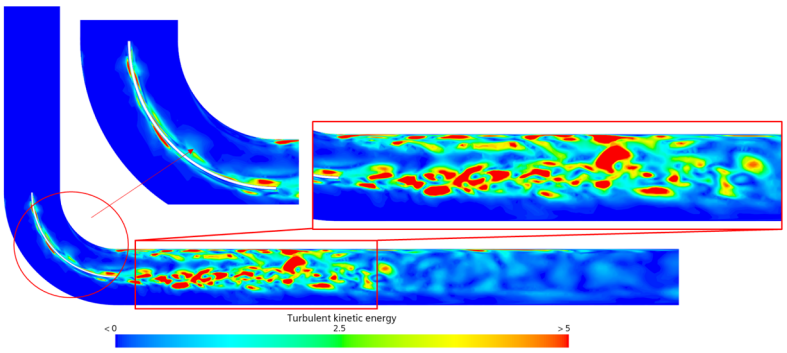

(a) The normal guide vane

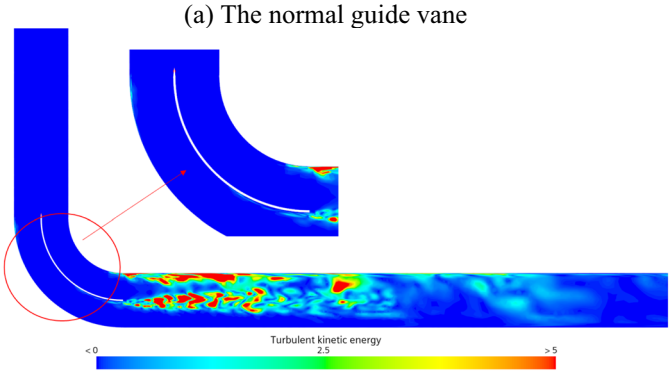

(b) The leading-edge serrated guide vane

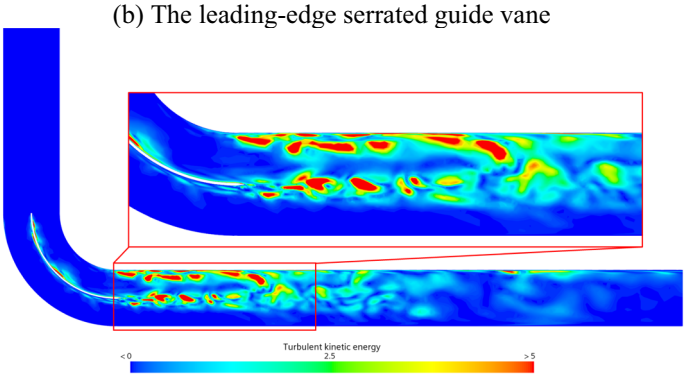

(c) The trailing-edge serrated guide vane

Fig. 16 Turbulent kinetic energy distribution of the elbows with the normal guide vane, the leading-edge serrated guide vane and the trailing-edge serrated guide vane in different parts

guide vane with leading-edge serrations is lower than that of the conventional guide vane. This suggests that the leading-edge serrations help streamline the flow field at the tip and both sides of the guide blade. Figure 16a, c shows that the turbulent kinetic energy downstream of the elbow fitted with the trailing-edge serrated guide vane is significantly reduced compared to that of the elbow with a standard guide vane. Consequently, pressure pulsations are also lower.

The vortex within the guide vane region of the elbow bend creates significant pressure fluctuations, contributing to aerodynamic noise on both the guide vane and the elbow bend. Analysis of the three different models reveals that both the leading-edge serrated guide vane and the trailing-edge serrated guide vane effectively streamline the internal airflow within the elbow, resulting in an improved flow field distribution in the elbow. Therefore, incorporating both leading-edge and trailing-edge serrated guide vanes is beneficial for noise reduction.

3.2 Sound Field Analysis

The fast Fourier transform (FFT) can be applied to extract sound source information from the unsteady simulation results. This enables the evaluation of the aerodynamic noise generated by the elbow with guide vanes.

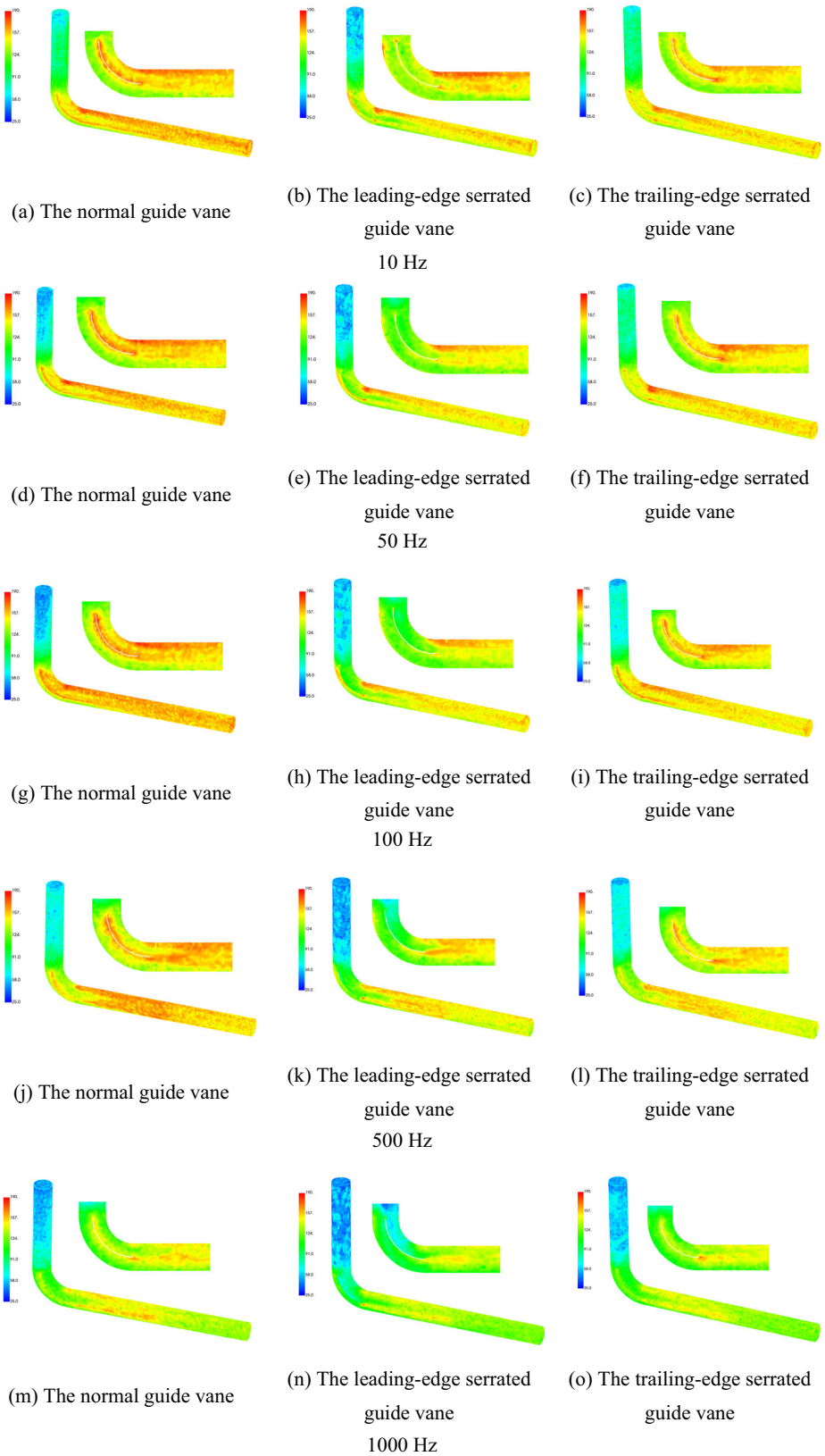

(a) The normal guide vane (b) The leading-edge serrated guide vane (c) The trailing-edge serrated guide vane

10 Hz

(d) The normal guide vane (e) The leading-edge serrated guide vane (f) The trailing-edge serrated guide vane

50 Hz

(g) The normal guide vane (h) The leading-edge serrated guide vane (i) The trailing-edge serrated guide vane

100 Hz

(j) The normal guide vane (k) The leading-edge serrated guide vane (l) The trailing-edge serrated guide vane

500 Hz

(m) The normal guide vane (n) The leading-edge serrated guide vane (o) The trailing-edge serrated guide vane

1000 Hz

Fig. 17 Distribution of dipole sound sources in the elbows with the normal guide vane, the leading-edge serrated guide vane and the trailing-edge serrated guide vane in different frequency range

Figure 17 illustrates the distribution of dipole sound sources in the elbow, considering the standard guide vane and the serrated guide vane. Table 4 presents information regarding the peak sound sources of the elbow at various frequencies, including 10 Hz, 50 Hz, 100 Hz, 500 Hz and 1000 Hz. Additionally, Table 5 delineates the reduction in sound source levels for the elbow equipped with the standard guide vane, the leading-edge serrated guide vane and the trailing-edge serrated guide vane. In comparison with the standard guide vane, those with the leading-edge serrated guide vane and trailing-edge serrated guide vane have not only fewer sound sources but also a narrower distribution range for these sources. The installation of both the leading-edge and trailing-edge serrated guide vanes, resulting in a more uniform flow field, is depicted in Figs. 15 and 16. Additionally, turbulence is effectively suppressed.

Figure 18 illustrates both the SPL and one-third octave. It is observed that elbows incorporating two serrated guide vanes exhibit lower levels of aerodynamic noise when compared to alternative designs. The graphical representation in

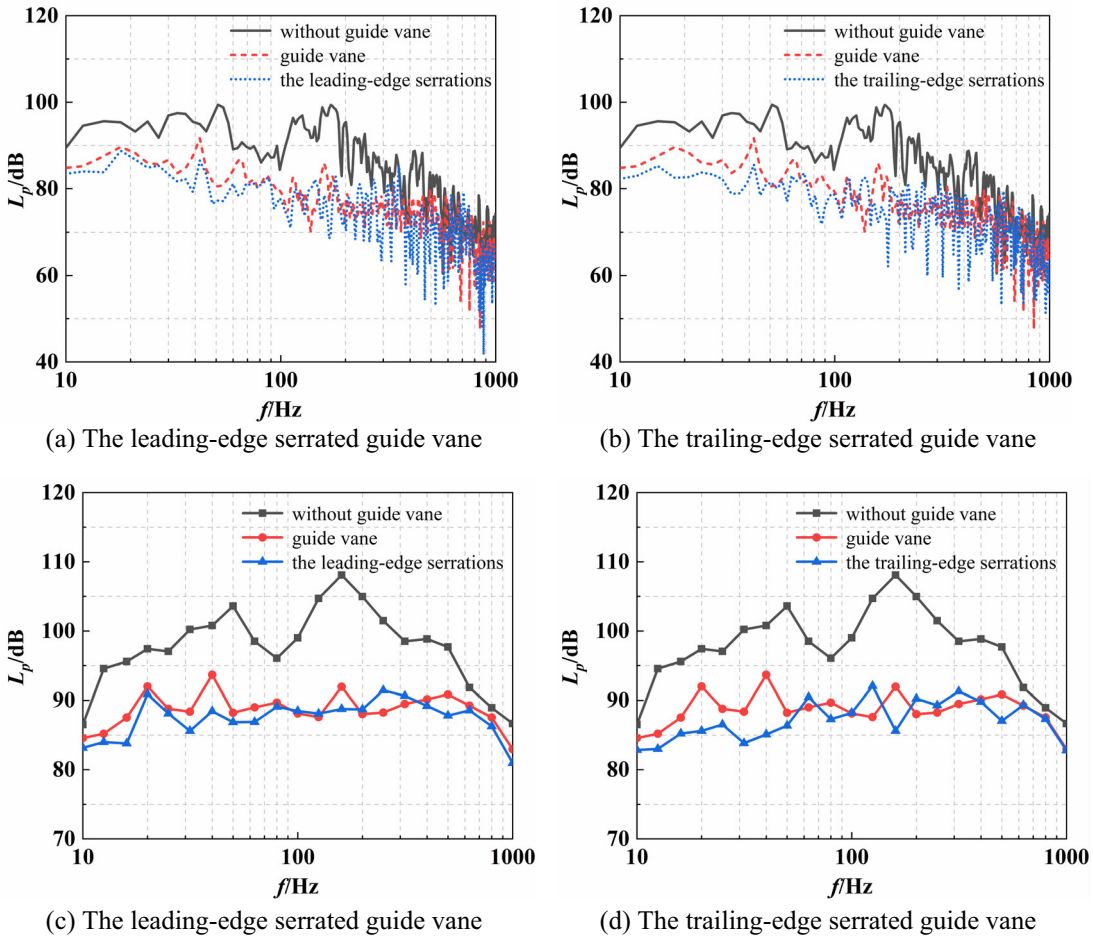

Fig. 18 Sound pressure level spectra of the leading-edge serrated guide vane and the trailing-edge serrated guide vane

Table 5 Comparison between the sound sources of bionic guide vanes and conventional guide vanes

Frequency (Hz)	10	50	100	500	1000
Elbow with a guide vane (dB)	188.3	191.5	189.2	179.5	172.7
Elbow with leading-edge serrated guide vane (dB)	184.5	189	183.1	175.4	168.7
Elbow with trailing-edge serrated guide vane (dB)	183.3	188.5	182.7	174.6	167.5
The reduction of the elbow with leading-edge serrated guide vane (dB)	3.8	2.5	6.1	4.1	4.0
The percentage of reduction	2.02%	1.31%	3.22%	2.28%	2.32%
The reduction of the elbow with a trailing-edge serrated guide vane (dB)	5.0	3.0	6.5	4.9	5.2
The percentage of reduction	2.65%	1.57%	3.43%	2.73%	3.01%

Table 6 Overall sound pressure levels of elbows with different guide vane

	Overall sound pressure level (dB)	The reduction (dB)	The reduction percent
Guide vane	115.2	–	–
Leading-edge serrated guide vane	110.5	4.7	4.08%
Trailing-edge serrated guide vane	111.6	3.6	3.13%

Fig. 17 consistently shows that the addition of the guide vane leads to a reduction in aerodynamic noise when contrasted with the standard elbow configuration. Additionally, the bionic structures show consistent improvement in aerodynamic noise reduction in comparison with the standard guide vane elbow, achieving an overall sound level reduction of up to 4.7 dB and 3.6 dB, with a maximum noise reduction of 7.27 dB (Table 6).

These results suggest that the leading-edge serrated guide vane and the trailing-edge serrated guide vane are highly effective in reducing aerodynamic noise in elbows, as supported by both numerical simulation and experimental data.

4 Conclusions

This paper explores the decrease in the aerodynamic noise in elbow configurations using a combination of computational and experimental research, with inspiration from bionic technology. To reduce aerodynamic noise in elbow constructions, leading-edge and trailing-edge serrated guide vanes have been introduced. The following conclusions are obtained:

(1) Both the numerical and experimental analyses demonstrated that the flow field of elbows with conventional guide vanes and serrated guide vanes can be analyzed using the mixed numerical approach. The results indicate that the mixed method have minimal calculation errors and presented advantages in the calculation of aerodynamic noise in elbows equipped with three different guide vanes.
(2) The analysis of the experiment also showed that the serrated guide vane is successful in lowering the aerodynamic noise. In the 0–5000 Hz range, the leading-edge serrated guide vane can reduce to 4.6 dB, while the trailing-edge serrated guide vane can lower to 3.4 dB.
(3) The numerical analysis has revealed that the leading-edge serrated guide vane and the trailing-edge serrated guide vane reduce the aerodynamic noise in elbows by effectively suppressing the generation of vortices at the top and tail of the guide vanes. This mechanism has been profoundly demonstrated, showing that the airflow inside the elbow becomes more uniform due to the presence of these serrated guide vanes.

Acknowledgements This work is financially supported by the National Natural Science Foundation of China (No. 51779201), the National Natural Science Foundation of China (No. 52271291), the National Natural Science Foundation of China (No. 5177090601), the Joint Fund of the Ministry of Education of China (6141A02022139) and the Nature Science Foundation of Hubei Province (ZRMS2020000207).

References

1. Hersh, A.S., Soderman, P.T., Hayden, R.E.: Investigation of acoustic effects of leading-edge serrations on airfoils. J. Aircr. **11**, 197–202 (1974). https://doi.org/10.2514/3.59219
2. Rao, C., Ikeda, T., Nakata, T., Liu, H.: Owl-inspired leading-edge serrations play a crucial role in aerodynamic force production and sound suppression. Bioinspir. Biomim. **12**, 046008 (2017). https://doi.org/10.1088/1748-3190/aa7013
3. Jones, L., Sandberg, R.: Acoustic and hydrodynamic analysis of the flow around an aerofoil with trailing-edge serrations. J. Fluid Mech. **706**, 295–322 (2012). https://doi.org/10.1017/jfm.2012.254
4. Avallone, F., Van, D., Ragni, D.: Benefits of curved serrations on broadband trailing-edge noise reduction. J. Sound Vib. **400**, 167–177 (2017). https://doi.org/10.1016/j.jsv.2017.04.007
5. Howe, M.S.: Aerodynamic noise of a serrated trailing edge. J. Fluids Struct. **5**, 33–45 (1991). https://doi.org/10.1016/0889-9746(91)80010-B
6. Howe, M.S.: Noise produced by a sawtooth trailing edge. Acoust. Soc. Am. J. **90**, 482–487 (1998). https://doi.org/10.1121/1.401273
7. Wang, L., Liu, X., Wu, L., Li, D.: Effect of the asymmetric bio-inspired trailing-edge serrations on sound suppression in a coupled owl-based airfoil. Appl. Acoust. **191**, 108667 (2022). https://doi.org/10.1016/j.apacoust.2022.108667
8. Kholodov, P., Moreau, S.: Optimization of trailing-edge serrations with and without slits for broadband noise reduction. J. Sound Vib. **490**, 115736 (2021). https://doi.org/10.1016/j.jsv.2020.115736
9. Arce León, C., Merino-Martínez, R., Pröbsting, S., Ragni, D., Avallone, F.: Acoustic emissions of semi-permeable trailing edge serrations. Acoust. Aust. **46**, 111–117 (2018). https://doi.org/10.1007/s40857-017-0093-8
10. Zhou, P., Liu, Q., Zhong, S., Fang, Y., Zhang, X.: A study of the effect of serration shape and flexibility on trailing edge noise. Phys. Fluids (2020). https://doi.org/10.1063/5.0032774
11. Singh, R., Mimani, A.: An aeroacoustics analysis on the effect of flexible trailing-edge modifications at large chord-based Reynolds number. In: Presented at the PROCEEDINGS of the 24th International Congress on Acoustics
12. Singh, R., Mimani, A.: Effect of flexible trailing-edge modifications on three-dimensional airfoil noise at large Reynolds numbers. In: Presented at the AIAA AVIATION 2023 Forum (2023)
13. Sivakumar, A., Porteous, R., Mimani, A., Doolan, C.J.: An experimental investigations of turbulent boundary-layer interaction with different serrated trailing-edge configurations. Hunter Valley Acoust. **2015**, 1–10 (2015)

14. Borelli, D., Gaggero, T., Rizzuto, E., Schenone, C.: Onboard ship noise: acoustic comfort in cabins. Appl. Acoust. **177**, 107912 (2021). https://doi.org/10.1016/j.apacoust.2021.107912
15. Li, Q., Song, J., Shang, D., Tang, R.: Sound radiation at the nozzle of a pipeline system and noise reduction based on a non-anechoic pool. Appl. Acoust. **182**, 108227 (2021). https://doi.org/10.1016/j.apacoust.2021.108227
16. Cinquemani, S., Braghin, F.: Decentralized active vibration control in cruise ships funnels. Ocean Eng. (2017). https://doi.org/10.1016/j.oceaneng.2017.06.008
17. Borelli, D., Gaggero, T., Rizzuto, E., Schenone, C.: Analysis of noise on board a ship during navigation and manoeuvres. Ocean Eng. **105**, 256–269 (2015). https://doi.org/10.1016/j.oceaneng.2015.06.040
18. Ahlborn, B., Groves, S.: Secondary flow in a vortex tube. Fluid Dyn. Res. **21**, 73–86 (1997). https://doi.org/10.1016/S0169-5983(97)00003-8
19. Uzun, A., Hussaini, M.Y.: Prediction of Noise generated by a round nozzle jet flow using computational aeroacoustics. J. Comput. Acoust. **19**, 291–316 (2011). https://doi.org/10.1142/S0218396X11004365
20. Masumoto, T., Mori, M., Yasuda, Y., Inoue, N., Sakuma, T.: Fast multipole boundary element method for aerodynamic sound field analysis based on lighthill's equation. J. Theor. Comput. Acoust. **31**, 2350009 (2023). https://doi.org/10.1142/S2591728523500093
21. Han, T., Wang, L., Cen, K., Song, B., Wang, Q.: Flow-induced noise analysis for natural gas manifolds using LES and FW-H hybrid method. Appl. Acoust. (2020). https://doi.org/10.1016/j.apacoust.2019.107101
22. Masaaki, M.: Takayuki, Masumoto, Kunihiko, Ishihara: study on acoustic, vibration and flow induced noise characteristics of T-shaped pipe with a square cross-section. Appl. Acoust. **120**, 137–147 (2017). https://doi.org/10.1016/j.apacoust.2017.01.022
23. Zhang, T., Zhang, Y.O., Ouyang, H.: Structural vibration and fluid-borne noise induced by turbulent flow through a 90° piping elbow with/without a guide vane. Int. J. Press. Vessels Pip. **125**, 66–77 (2015). https://doi.org/10.1016/j.ijpvp.2014.09.004
24. Zhang, Y.O., Zhang, T., Ouyang, H., Li, T.Y.: Flow-induced noise analysis for 3D trash rack based on LES/Lighthill hybrid method. Appl. Acoust. **141**, 152 (2014). https://doi.org/10.1016/j.apacoust.2013.12.016
25. Wang, X., Li, N., Yu, M., Lin, H., Ye, L.: Research on acoustic behaviors of water pipelines with guide vanes. J. Vib. Control **29**, 1280–1291 (2023). https://doi.org/10.1177/10775463211062338
26. Zhang, C., Luo, Y., Liang, J., Li, L., Li, J.: Flow-induced noise prediction for 90° bend pipeby LES and FW-H hybrid method. Sci. Res. Essays (2014). https://doi.org/10.5897/sre2014.5875
27. Li, M., Wu, J.H., Yuan, X.Y.: Wall suction & slip effect of spherical-grooved bionic metasurface for controlling the aerodynamic noise. Appl. Acoust. **171**, 107537 (2021). https://doi.org/10.1016/j.apacoust.2020.107537
28. Ye, J., Xu, M., Xing, P., Cheng, Y., Meng, D., Tang, Y., Zhu, M.: Investigation of aerodynamic noise reduction of exterior side view mirror based on bionic shark fin structure. Appl. Acoust. **182**, 108188 (2021). https://doi.org/10.1016/j.apacoust.2021.108188
29. Paruchuri, C., Joseph, P., Chong, T.P., Priddin, M.J., Ayton, L.: On the noise reduction mechanisms of porous aerofoil leading edges. J. Sound Vib. **485**, 115574 (2020). https://doi.org/10.1016/j.jsv.2020.115574
30. Lu, W., Zheng, G.: Passive control on deep cavity noise at subsonic speeds by leading-edge grooves. J. Vib. Control (2023). https://doi.org/10.1177/10775463231182256
31. Wei, Y., Qian, Y., Bian, S., Xu, F., Kong, D.: Experimental study of the performance of a propeller with trailing-edge serrations. Acoust. Aust. (2021). https://doi.org/10.1007/s40857-021-00221-w
32. Tan, L., Zhu, B., Wang, Y., Cao, S., Liang, K.: Turbulent flow simulation using large eddy simulation combined with characteristic-based split scheme. Comput. Fluids **94**, 161–172 (2014). https://doi.org/10.1016/j.compfluid.2014.01.037
33. Ferziger, J.H., Perić, M.: Computational Methods for Fluid Dynamics. Springer, Berlin (2002)
34. Goldstein, M.: Unified approach to aerodynamic sound generation in the presence of solid boundaries. J. Acoust. Soc. Am. **56**, 497–509 (1974). https://doi.org/10.1121/1.1903283
35. Ye, L., Wang, X., Wu, W., Ma, H., Li, N.: Study on acoustic characteristics of air pipeline with guide vane and bionic guide vane. Ocean Eng. **284**, 115197 (2023). https://doi.org/10.1016/j.oceaneng.2023.115197
36. Chen, S.-S.: Flow-induced vibration of circular cylindrical structures. Argonne National Lab.(ANL), Argonne (1985)
37. Jeong, S.J., Kim, W.S.: A study on the optimal monolith combination for improving flow uniformity and warm-up performance of an auto-catalyst. Chem. Eng. Process. **42**, 879–895 (2003). https://doi.org/10.1016/S0255-2701(02)00140-X
38. Zhu, J.J., Liu, G.W.: Numerical optimization for aerodynamic noises of rear view mirrors of vehicles based on rectangular cavity structures. J. Vibroeng. **20**, 1240–1256 (2018). https://doi.org/10.21595/jve.2017.18740